Ladder-Type Pentaphenylene Dyes for Dye-Sensitized Solar Cells

Gang Zhou,[†] Neil Pschirer,[‡] Jan C. Schöneboom,[‡] Felix Eickemeyer,[‡] Martin Baumgarten,[†] and Klaus Müllen*,[†]

Max-Planck-Institute for Polymer Research, Ackermannweg 10, Mainz D-55128, Germany, and BASF AG, D-67056, Ludwigshafen, Germany

Received August 28, 2007

A series of donor−π-acceptor dyes based on rigid ladder-type pentaphenylene spacers **1**–**3** have been synthesized from dibromopentaphenylene **4** in three steps. The three dyes contain the same acceptors (2-cyanoacrylic acid) as anchor groups but differ in donor units (diphenylamino **1**, phenothiazinyl **2**, and bis(*N*,*N*-4-dimethylaminophenyl)amino **3**). Their maximum absorption peaks range from 442 to 457 nm with high extinction coefficients, while dye **3** shows a broader absorption band in the visible region along with a weak NIR absorption band due to the formation of amino radical cation. The DSSCs based on these dyes demonstrate the highest IPCE value of 73% and power conversion efficiency of 2.3% (liquid cell) and 0.8% (solid cell), respectively. Although the power conversion efficiencies are not so high, this work explores new donor−spacer−acceptor models and the effects of molecular design on photophysical and photoelectrochemical properties.

Introduction

Since the discovery by Grätzel in 1991,[1] dye-sensitized solar cells (DSSCs) have attracted a great deal of interest due to their low cost and relatively high power conversion efficiency (η).[2] Until now, Ru−bipyridine complex[3] sensitized TiO_2 electrodes have shown the highest η values (9–11%). However, in view of cost and limited availability of ruthenium complexes, metal-free organic dyes are strongly desired due to the following reasons:[4] (1) they have larger absorption coefficients (attributed to an intramolecular $\pi-\pi^*$ transition) than metal complex photosensitizers (attributed to metal-to-ligand charge transfer absorption), leading to efficient light-harvesting properties; (2) the varieties in their structures provide possibilities for molecular design, e.g., the introduction of substituents, and thus allow for easy control of their absorption spectra; (3) there are no concerns about environmental demand because organic dyes do not contain expensive noble metals, such as ruthenium.

A typical DSSC comprises a dye-sensitized nanocrystalline porous metal oxide film, such as TiO_2,[5] interpenetrated by a hole-transporting material (HTM), such as a liquid electrolyte containing an I^-/I_3^- redox couple.[6] Absorption of light by the sensitizer creates a high-energy state that can inject the photoexcited electron into the conduction band of TiO_2. The oxidized dye is subsequently reduced back to the ground state by electron transfer from an I^-/I_3^- redox couple or from HTM in film pores. Efficient operation of the DSSC devices relies upon the minimization of the possible recombination pathways occurring between electrons in TiO_2 and (1) a dye cation or (2) HTM.[7] For effective solar energy conversion, it is essential to establish the conditions of high electron injection efficiency and effective charge separation for slow recombination.[8]

* Corresponding author. E-mail: muellen@mpip-mainz.mpg.de.
[†] Max-Planck-Institute for Polymer Research.
[‡] BASF AG.

(1) O'Regan, B.; Grätzel, M. *Nature (London)* **1991**, *353*, 737.
(2) (a) Grätzel, M. *Nature (London)* **2001**, *414*, 338. (b) Tian, H.; Yang, X.; Chen, R.; Pan, Y.; Li, L.; Hagfeldt, A.; Sun, L. *Chem. Commun.* **2007**, 3741. (c) Mwaura, J. K.; Zhao, X.; Jiang, H.; Schanze, K. S.; Reynolds, J. R. *Chem. Mater.* **2006**, *18*, 6109. (d) Schmidt-Mende, L.; Kroeze, J. E.; Durrant, J. R.; Nazeeruddin, Md. K.; Grätzel, M. *Org. Lett.* **2005**, *5*, 1315. (e) Chen, R.; Yang, X.; Tian, H.; Wang, X.; Hagfeldt, A.; Sun, L. *Chem. Mater.* **2007**, *19*, 4007. (f) Grätzel, M. *Chem. Lett.* **2005**, *34*, 8. (g) Hara, K.; Kurashige, M.; Ito, S.; Shinpo, A.; Suga, S.; Sayama, K.; Arakawa, H. *Chem. Commun.* **2003**, 252. (h) Tokuhisa, H.; Hammond, P. T. *Adv. Funct. Mater.* **2003**, *13*, 831. (i) Horiuchi, T.; Miura, H.; Sumioka, K.; Uchida, S. *J. Am. Chem. Soc.* **2004**, *126*, 12218. (j) Li, S. L.; Jiang, K. J.; Shao, K. F.; Yang, L. M. *Chem. Commun.* **2006**, 2792. (k) Kim, S.; Lee, J. K.; Kang, S. O.; Ko, J.; Yum, J. H.; Fantacci, S.; De Angelis, F.; Di Censo, D.; Nazeeruddin, M. K.; Grätzel, M. *J. Am. Chem. Soc.* **2006**, *128*, 16701. (l) Hara, K.; Sayama, K.; Arakawa, H.; Ohga, Y.; Shinpo, A.; Suga, S. *Chem. Commun.* **2001**, 569–570. (m) Kurashige, Y.; Nakajima, T.; Kurashige, S.; Hirao, K.; Nishikitani, Y. *J. Phys. Chem. A* **2007**, *111*, 5544. (n) Sayama, K.; Sugino, M.; Sugihara, H.; Abe, Y.; Arakawa, H. *Chem. Lett.* **1998**, 753.
(3) (a) Nazeeruddin, M. K.; Kay, A.; Rodicio, I.; Baker, R. H.; Müller, E.; Kiska, P.; Vlachopoulos, N.; Grätzel, M. *J. Am. Chem. Soc.* **1993**, *115*, 6382. (b) Nazeeruddin, M. K.; Péchy, P.; Renouard, T.; Zakeeruddin, S. M.; Humphry-Baker, R.; Comte, P.; Liska, P.; Cevey, L.; Costa, E.; Shklover, V.; Spiccia, L.; Deacon, G. B.; Bignozzi, C. A.; Grätzel, M. *J. Am. Chem. Soc.* **2001**, *123*, 1613. (c) Nazeeruddin, M. K.; Zakeeruddin, S. M.; Humphry-Baker, R.; Jirousek, M.; Liska, P.; Vlachopoulos, N.; Shklover, V.; Fischer, C.-H.; Grätzel, M. *Inorg. Chem.* **1999**, *38*, 6298. (d) Gregg, B. A. *J. Phys. Chem. B* **2003**, *107*, 4688. (e) Nazeeruddin, M. K. *Coord. Chem. Rev.* **2004**, *248*, 1161. (f) Ito, S.; Zakeeruddin, S. M.; Humphry-Baker, R.; Liska, P.; Charvet, R.; Comte, P; Nazeeruddin, M.; K.; Péchy, P.; Takata, M.; Miura, H.; Uchida, S.; Grätzel, M. *Adv. Mater.* **2006**, *18*, 1202. (g) Durrant, J. R.; Haque, S. A.; Palomares, E. *Chem. Commun.* **2006**, 3279. (h) Chiba, Y.; Islam, A.; Watanabe, Y. Y.; Komiya, R.; Koide, N.; Han, L. *Jpn. J. Appl. Phys.* **2006**, *45*, L638.
(4) (a) Hara, K.; Sata, R.; Katoh, R.; Furube, A.; Ohga, Y.; Shinpo, A.; Suga, S.; Sayama, K.; Sugihara, H.; Arakawa, H. *J. Phys. Chem. B* **2003**, *107*, 597. (b) Sayama, K.; Tsukagoshi, S.; Hara, K.; Ohga, Y.; Shinpou, A.; Abe, Y.; Suga, S.; Arakawa, H. *J. Phys. Chem. B* **2002**, *106*, 1363.
(5) Vlachopoulos, N.; Liska, P.; Augustynski, J.; Grätzel, M. *J. Am. Chem. Soc.* **1998**, *110*, 1216.
(6) Hagfeldt, A.; Grätzel, M. *Acc. Chem. Res.* **2000**, *33*, 269.
(7) Kalyanasundaram, K.; Grätzel, M. *Micelles, Microemulsions, Monolayers, Int. Symp.* **1998**, 579.

10.1021/cm703459p CCC: $40.75
Published on Web 02/19/2008

Scheme 1. Synthetic Route of Compounds 1–3

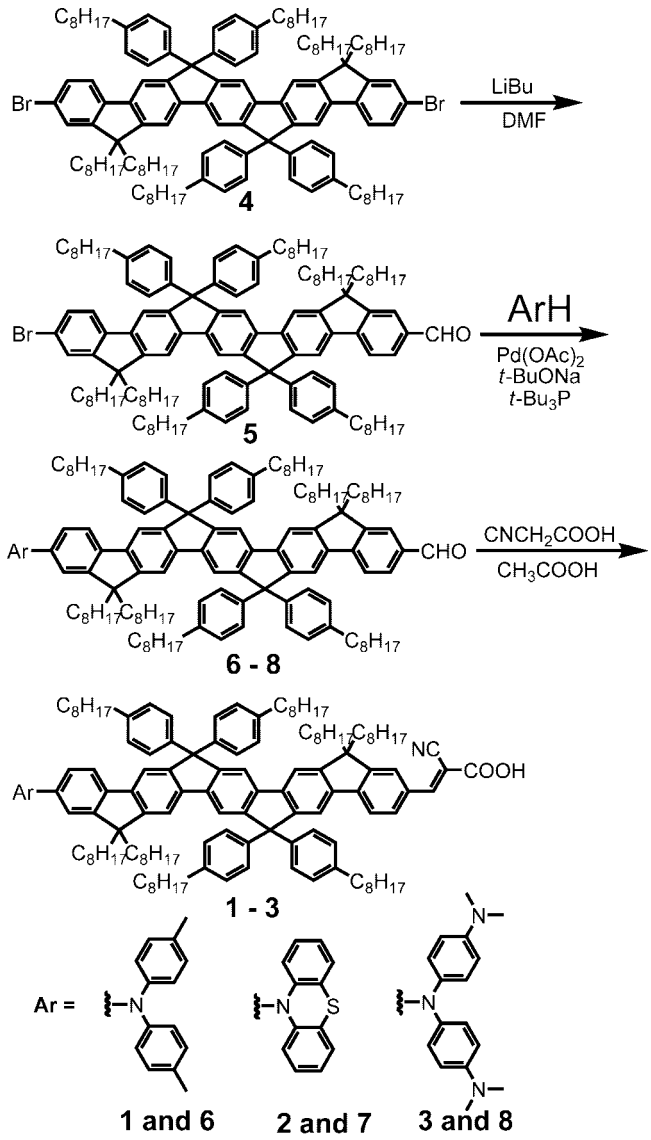

Herein, we present the synthesis and solar cell performance of three D−π−A chromophores **1**–**3** with the chemical structures shown in Scheme 1. In these dyes, arylamine derivatives act as electron donors (D) and 2-cyanoacrylic acetic acid acts as an electron acceptor (A) and anchoring group for attachment to the TiO_2. The donors and acceptors are bridged by ladder-type pentaphenylenes with orbital partitioning, which was revealed by density functional theory calculations (B3LYP/def-SV(P)),[9] as shown in Figure 1. The highest occupied molecular orbital (HOMO) localizes on the arylamine moiety, and the lowest unoccupied molecular orbital (LUMO) localizes on the cyanoacrylic group without overlapping the HOMO, which illustrates that the HOMO and LUMO are completely separated. Therefore, photoexcitation may lead to an efficient intramolecular charge separation[10] with an effective photocurrent generation and slow recombination. Furthermore, the bulky alkylphenyl groups could suppress the aggregation due to the disturbance of the $\pi-\pi$ stacking, which should always be avoided for efficient photocurrent generation because aggregation may lead to intermolecular quenching or affect the light absorption by the filtering effect.[11]

Results and Discussion

Synthesis and Structure Characterization. The straightforward synthetic routes to the three pentaphenylene derivatives are depicted in Scheme 1. The synthesis begins with alkyl- and aryl-substituted ladder-type dibromopentaphenylene **4** which was previously developed in our laboratory.[12] Lithiation of compound **4** with a stoichiometric amount of *n*-butyllithium at −78 °C followed by quenching with dimethylformamide and subsequent acidic hydrolysis produced the corresponding monoaldehyde-substituted pentaphenylene derivatives **5**. The subsequent arylamination of aldehyde **5** was readily performed in the presence of palladium acetate and a nonnucleophilic base, Cs_2CO_3 being the most suitable.[13] In the last step, the aldehyde derivatives **6**–**8** were converted to the dyes **1**–**3** by reaction with cyanoacetic acid in refluxing acetic acid in the presence of ammonium acetate. The target compounds were characterized by NMR spectroscopy, elemental analysis, and mass spectrometry and were found to be consistent with the proposed structures. The obtained dyes are dark red or orange in the solid state and freely dissolve in dichloromethane (DCM) to produce a red solution.

Optical Properties. The UV–vis−NIR absorption spectra recorded for the DCM solution (ca. 10^{-5} M) of the dyes **1**–**3** are displayed in Figure 2. All the dyes exhibit main absorption peaks around 442−457 nm with extinction coefficients above 7×10^4 M^{-1} cm^{-1} due to the $\pi-\pi^*$ transition of the chromophore backbones. Compared with the absorption of compound **1**, the absorption spectrum of compound **2** shows a 15 nm hypsochromic shift. This could be probably due to the nonplanar structure of phenothiazine, which decreases the effective conjugation of the molecules.[14] While compound **3** exhibits the main absorption band at 444 nm, the corresponding peak is slightly broader than those for dyes **1** and **2**. However, compound **3** displays a weak absorption peak at 1040 nm in DCM and chloroform solutions with extinction coefficient of 1.04×10^4 and 1.91×10^4 M^{-1} cm^{-1}, respectively (Figure 3). No obvious band in the NIR region was observed in the absorption spectra of compound **3** in more polar solvents, such as tetrahydrofuran (THF) and *N*,*N*-dimethylformamide (DMF), while they exhibit almost the same absorption maximum around 444

(8) Ramakrishna, G.; Singh, A. K.; Palit, D. K.; Ghosh, H. N. *J. Phys. Chem. B* **2004**, *108*, 12489.
(9) (a) Ahlrichs, R.; Bär, M.; Häser, M.; Horn, H.; Kölmel, C. *Chem. Phys. Lett.* **1989**, *162*, 165. (b) Becke, A. D. *J. Chem. Phys.* **1993**, *98*, 5648. (c) Lee, C.; Yang, W.; Parr, R. G. *Phys. Rev. B* **1988**, *37*, 785. (d) Schäfer, A.; Horn, H.; Ahlrichs, R. *J. Chem. Phys.* **1992**, *97*, 2571.
(10) Oseki, Y.; Fujitsuka, M.; Cho, D. W.; Sugimoto, A.; Tojo, S.; Majima, T. *J. Phys. Chem. B* **2005**, *109*, 19257.
(11) (a) Liu, D.; Fessenden, R. W.; Hug, G. L.; Kamat, P. V. *J. Phys. Chem. B* **1997**, *101*, 2583. (b) Wang, Z. S.; Li, F. Y.; Huang, C. H.; Wang, L.; Wei, M.; Jin, L. P.; Li, N. Q. *J. Phys. Chem. B* **2000**, *104*, 9676.
(12) Jacob, J.; Sax, S.; Piok, T.; List, E. J. W.; Grimsdale, A. C.; Müllen, K. *J. Am. Chem. Soc.* **2004**, *126*, 6987.
(13) Chiang, C. L.; Wu, M. F.; Dai, D. C.; Wen, Y. S.; Wang, J. K.; Chen, C. T. *Adv. Funct. Mater.* **2005**, *15*, 231.
(14) Sun, D.; Rosokha, S. V.; Kochi, J. K. *J. Am. Chem. Soc.* **2004**, *126*, 1388.

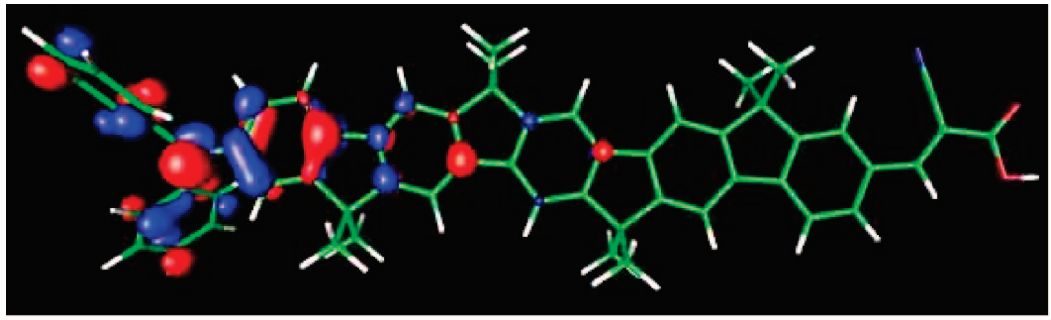

HOMO

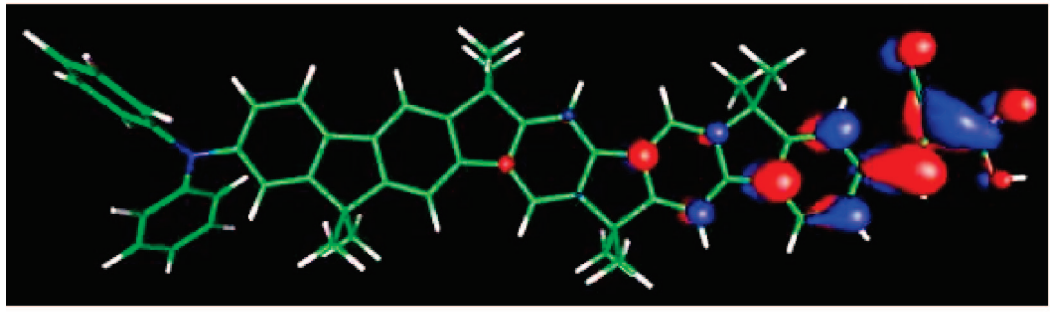

LUMO

Figure 1. Plots of HOMO and LUMO of dye **1** from B3LYP/def-SV(P) calculation. Plot generated with gOpenMol (Leif Laaksonen, Center for Scientific Computing, Espoo, Finland, http://www.csc.fi/gopenmol/).

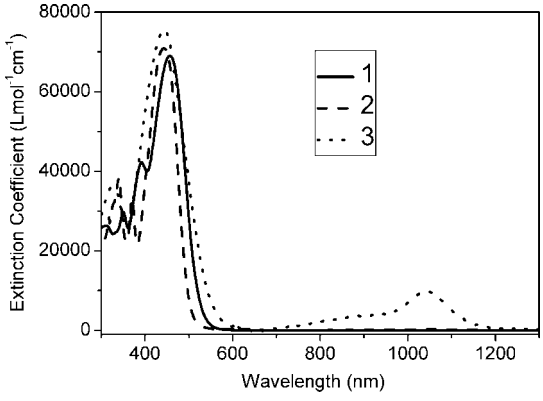

Figure 2. UV–vis−NIR absorption spectra of dyes **1–3** in DCM solutions.

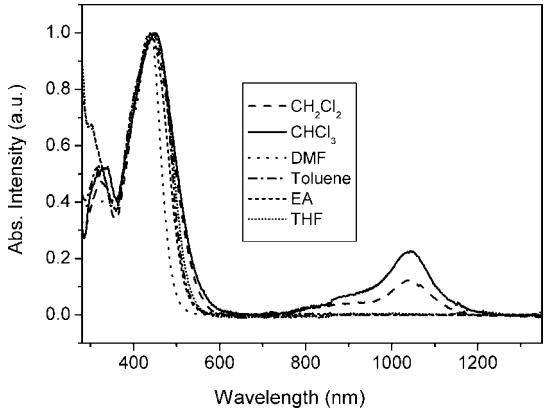

Figure 3. UV–vis−NIR absorption spectra of dye **3** in different solvents.

nm (Figure 3). However, when the solution of compound **3** in DCM or chloroform was treated with hydrazine, the NIR absorption band completely disappeared while the absorption

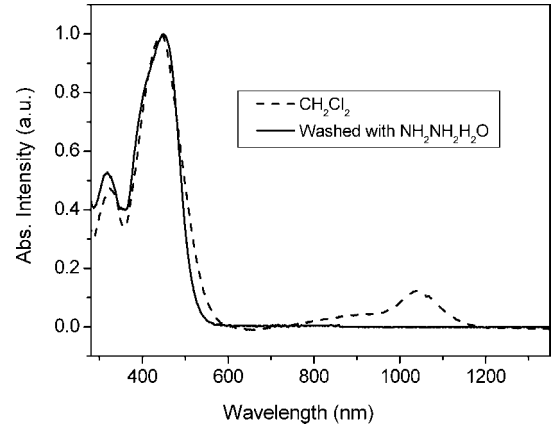

Figure 4. UV–vis−NIR absorption spectra of dye **3** before and after treated with hydrazine.

band around 444 nm was almost identical (Figure 4). This result indicates that the absorption peak in the NIR region could be attributed to the radical cation of the amine moiety which was formed from oxidation by the trace of impurity in the solvents and could be reduced by hydrazine. The absorption band in the NIR region of an amino radical cation was also found in our previous work.[15]

The dyes can be adsorbed on TiO_2 films from a variety of solutions because of the presence of a carboxylic group in the molecules. For comparison, the absorption spectra of the adsorbed dyes on TiO_2 are shown in Figure 5. When the dye is attached to TiO_2, a 23–37 nm hypsochromic shift of the absorption maximum was observed for dyes **1–3**, and it

(15) Zhou, G.; Baumgarten, M.; Müllen, K. *J. Am. Chem. Soc.* **2007**, *129*, 12211.

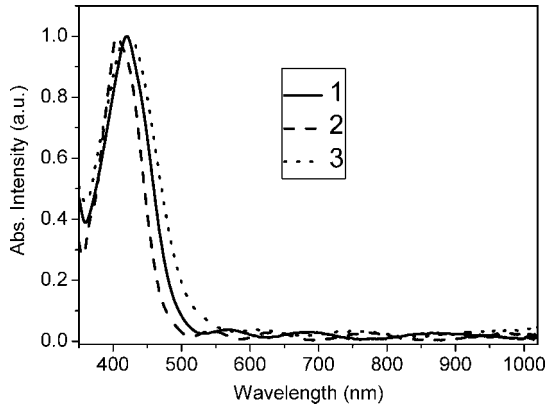

Figure 5. UV–vis−NIR absorption spectra of dyes **1**–**3** after binding onto TiO_2.

does not change when adding DCM on the dye−TiO_2 slide. Such a hypsochromic shift of the absorption spectrum has also been observed for other organic dyes.[16] It could be interpreted as a polar interaction and/or deprotonation of the dyes by adsorption on the TiO_2 surface.

Electrochemical Properties. The electrochemical behavior of the diamines **1**–**3** was investigated by cyclic voltammetry (CV), and all data are summarized in Table 1. The CV measurements were performed in a solution of Bu_4NPF_6 (0.1 M) in water-free dichloromethane with a scan rate of 50 mV/s at room temperature under argon. A platinum electrode was used as the working electrode and ferrocene as the reference.

All the dyes are redox-stable, exhibiting reversible oxidation couples which are required for sustaining dye-sensitized solar cells. As shown in Figure 6, the oxidation onset of compounds **1** and **2** are almost the same, which is attributed to the oxidation of diphenylamine and phenothiazine. The second and the third oxidation couples correspond to the electron removal from pentaphenylenes,[15] which indicates that the dyes can be reversibly oxidized at moderately high oxidation potentials more positive than I^-/I_3^- redox couples (0.42 V vs NHE).[17] An oxidation potential higher than that of the iodine couple is necessary to ensure that the neutral dye is regenerated after it has injected its electron into the TiO_2 layer.[18] The reversibility of the oxidation couple is indicative of a high stability of the dye under operating conditions of the device.

The corresponding oxidation couples of dye **3** at high potential are almost the same as those for dyes **1** and **2**. However, dye **3** displays a first oxidation couple at 0.48 V vs NHE due to the oxidation of the *N*,*N*-dimethylphenylamine. This also indicates that the two amino groups could be easily oxidized into their radical cations, as already found in its absorption spectrum. For dyes **1** or **2**, the first oxidation potential is much higher, which induces the absence of the formation of the amino radical cation and the NIR absorption. Compared with the oxidation potential of triarylamine in dye **1**, the half-wave oxidation potential for the triarylamine group in dye **3** shifts negatively to 0.96 V due to the electron donation from the two *N*,*N*-dimethylamine groups. From the potential of the oxidation onset, the HOMOs of three dyes can be estimated according to equation $E_{HOMO} = -(E^{OX} + 4.2)$,[19] and then the corresponding LUMOs of the three dyes can be calculated by subtraction of the optical band gap from the E_{HOMO}. All the data are listed in Table 1.

Photovoltaic Properties. The dye-sensitized solar cells were constructed using these dyes as a sensitizer for nanocrystalline anatase TiO_2 on FTO in two different types, namely liquid and solid solar cells. The current–voltage characteristics were measured under simulated solar irradiation (1 sun = 100 mW/cm 1.5 air mass global), as shown in Figure 7, and the device performance statistics are listed in Table 2.

The first type is liquid solar cells, and they were fabricated with 0.5 M LiI/0.25 M *n*-Bu_4NI/0.05 M I_2 in acetonitrile solutions as electrode. Action spectra of the incident photon-to-current conversion efficiency (IPCE) as a function of wavelength were measured to evaluate the photoresponse in the whole region, and the data are plotted in Figure 8. High IPCE performance (above 60%) was observed in the range from 400 to 520 nm for dyes **1** and **2**, with maximum values of 68% at 480 nm and 73% at 460 nm. The η value of the cell based on dye **1** (2.3%) is larger than that of the cell based on dye **2** (1.8%). The difference in performance between the diphenylamine-substituted dye **1** and phenothiazine-substituted dye **2** probably stems from the bathochromic shift in the absorption spectrum of dye **1**. However, although dye **3** shows a broader absorption spectrum which covers the whole absorption region of dyes **1** and **2**, the maximum IPCE value is 56% at 440 nm, and the η value is only 1.0%. We attribute this relatively low efficiency to poor regeneration of the oxidized dye **3**. According to the energy level diagram shown in Figure 9, the HOMO potentials of dye **1** as well as of dye **2** are suitable for electron transfer from I^- (1.07 and 1.06 eV vs NHE), whereas that of dye **3** has a too low potential, which results in a lower overall device performance.

Solid dye-sensitized solar cells (sDSSCs) were fabricated by spin-coating a solution of 0.16 M 2,2′,7,7′-tetrakis(*N*,*N*-di-*p*-methoxyphenylamine)-9,9′-spirobifluorene (spiro-OMeTAD), 15 mM $LiN(SO_2CF_3)_2$, and 60 mM 4-*tert*-butylpyridine in chlorobenzene as a hole-transport layer between the dye and the metal electrode. Figure 10 displays the current–voltage curves of the sDSSCs based on dyes **1**–**3**. The relatively low fill factor of the cell based on dye **1** could probably be attributed to the different chemical structure, since the differences in the dye structures, especially the donors, have a significant influence on the wetting behavior with the spiro-MeO-TAD and, hence, pore filling. Furthermore, pore filling has an impact on shunt, series resistances, electron and hole lifetimes, and therefore on the fill factor. In our case, dye **1** has a different donor structure compared with dye **2**. Thus, they could have different wetting behavior

(16) (a) Hagberg, D. P.; Edvinsson, T.; Marinado, T.; Boschloo, G.; Hagfeldt, A.; Sun, L. *Chem. Commun.* **2006**, 2245. (b) Hara, K.; Wang, Z.-S.; Sato, T.; Furube, A.; Katoh, R.; Sugihara, H.; Dan-oh, Y.; Kasada, C.; Shinpo, A.; Suga, S. *J. Phys. Chem. B* **2005**, *109*, 15476.
(17) Hagfeldt, A.; Grätzel, M. *Chem. Rev.* **1995**, *95*, 49.
(18) Thomas, K. R. J.; Lin, J. T.; Hsu, Y. C.; Ho, K. C. *Chem. Commun.* **2005**, 4098.
(19) Bard A. J.; Faulkner, L. A. *Electrochemical Methods—Fundamentals and Applications*; Wiley: New York, 1984.

Table 1. Optical and Electrochemical Properties of Dyes 1–3 in DCM Solutions and Adsorbed on TiO_2

dye	λ_{max}^{Abs}, nm[a]	λ_{max}^{Abs}, nm[b]	ϵ 10^4, M^{-1} cm^{-1}	band gap exp (calc), eV	E_{onset}^{ox}, V (vs NHE)	HOMO exp (calc), eV	LUMO exp (calc), eV
1	457	420	6.90	2.36 (2.64)	1.07	−5.27(−5.12)	−2.91 (−2.48)
2	442	405	7.08	2.48 (2.49)	1.06	−5.26 (−5.20)	−2.78 (−2.71)
3	444	421	7.56	2.24 (2.38)	0.48	−4.68 (−4.47)	−2.44(−2.09)

[a] Absorption maxima of dyes **1–3** in DCM solutions (ca. 10^{-5} M). [b] Absorption maxima of dyes **1–3** adsorbed on TiO_2.

Table 2. Photovoltaic Performance of DSSCs Constructed with Dyes 1–3[a,b]

	liquid cell					solid cell			
dye	$IPCE_{max}$, %	V_{oc}, mV	J_{sc}, mA/cm^2	FF, %	η, %	V_{oc}, mV	J_{sc}, mA/cm^2	FF, %	η, %
1	68	522	8.57	52	2.3	552	3.41	31	0.6
2	73	526	6.83	50	1.8	546	3.31	42	0.8
3	56	478	5.14	43	1.1	330	0.15	34	0.02
N719		670	11.51	70	4.6				

[a] Thickness of the TiO_2 film: 10 μm (liquid cell); 2 μm (solid cell). [b] Devices were made without scattering layers, $TiCl_4$ treatment, and antireflecting coatings.

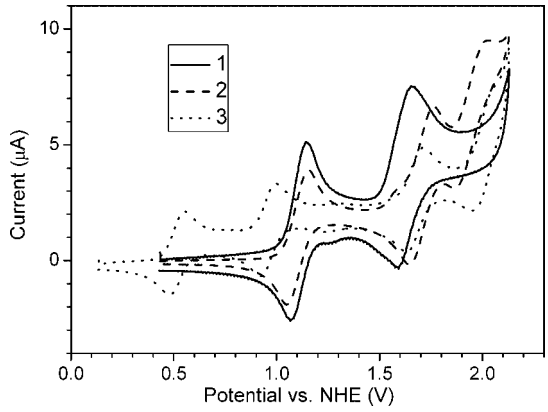

Figure 6. Cyclic voltammograms of dyes **1–3**.

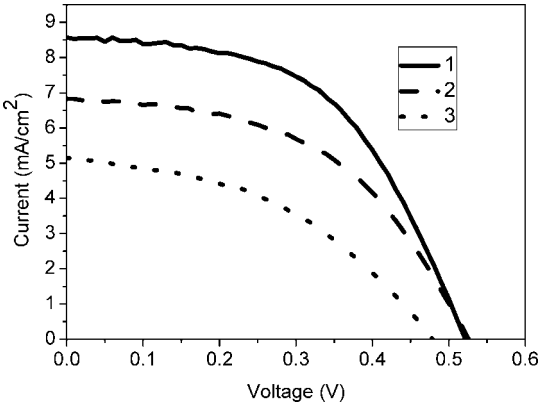

Figure 7. *I*−*V* curves of liquid cells based on dyes **1–3**.

and pore filling, which results in the different fill factor. The η values for DSSCs based on dyes **1**, **2**, and **3** are found to be 0.6%, 0.8%, and 0.02%, respectively. The differences in efficiencies of dyes **1** and **2** are within the reproducibility error of our experimental setup for solid-state solar cells. For the cell based on dye **3**, the hole transfer from the dye cation to spiro-OMeTAD is apparently inefficient due to the higher HOMO level of dye **3** than that of spiro-OMeTAD (0.73 V vs NHE),[20] which results in a rather poor efficiency. The reproducibility in sDSSCs is about 20% (i.e., Isc, Voc, FF, efficiency deviate by 20% between similar experiments) since pore filling (p-conductor in TiO_2) is very sensitively

(20) Handa, S.; Wietasch, H.; Thelakkat, M.; Durrant, J. R.; Haque, S. A. *Chem. Commun.* **2007**, 1725.

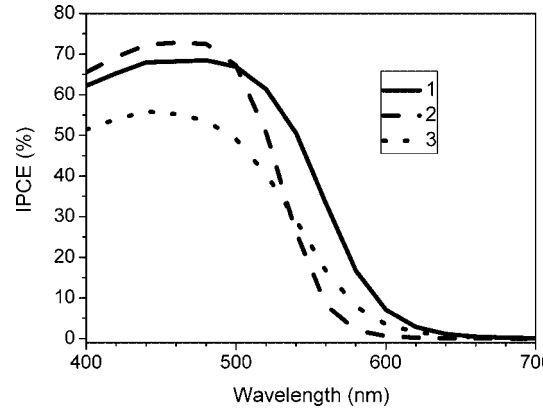

Figure 8. IPCE spectra for liquid DSSCs based on dyes **1–3**.

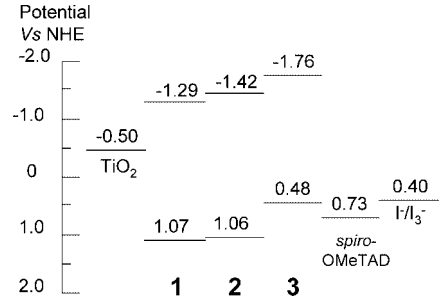

Figure 9. Schematic energy diagram for DSSCs based on dyes **1–3**.

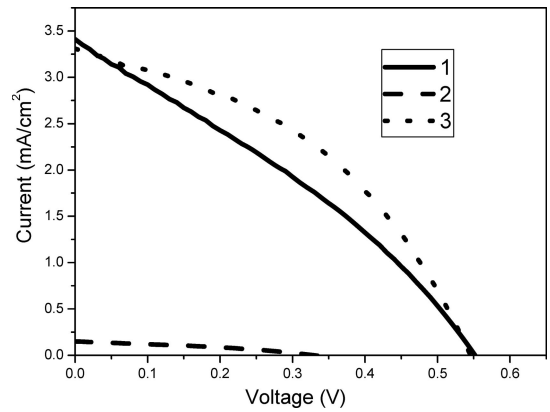

Figure 10. *I*−*V* curves for solid cells based on dyes **1–3**.

depending on preparation conditions (like ambient atmosphere). This is worse than in liquid cells, but it is a known phenomenon in the community and has not been solved yet.

Conclusions

In summary, three ladder-type pentaphenylene-based dyes with the same acceptor (2-cyanoacrylic acid) and different donors (diphenylamino **1**, phenothiazinyl **2**, and bis(*N*,*N*-4-dimethylaminophenyl)amino **3**) have been synthesized in three steps from dibromopentaphenylene. The maximum absorption peaks of the three dyes ranged from 442 to 457 nm with high extinction coefficients. Compared with dyes **1** and **2**, dye **3** shows a broader absorption band in the visible region along with a weak absorption band in the NIR region due to the formation of radical cation. The DSSCs based on these dyes demonstrate the highest IPCE value of 73% and power conversion efficiency of 2.3% (liquid cell) and 0.8% (solid cell), respectively. These results are comparable to some other dyes with maximum absorption around 600 nm,[21] which suggests that increasing the distance of the spacer between the donor and acceptor moieties is an effective approach to facilitate the charge separation for slow electron–hole recombination. This promising design opens up the possibility of novel sensitizers based on long spacer bridged donor and acceptors. Our future work is focused on the introduction of chromophores to bathochromic shift the absorption and to control the energy levels.

Experimental Section

Measurement and Characterization. ^{1}H and ^{13}C NMR spectra were recorded on a Bruker AMX 300 NMR (300 and 75 MHz, respectively) with dichloromethane-*d* or TDF-*d* as solvents and tetramethylsilane as internal standard. Chemical shifts are reported in parts per million. FD mass spectra were performed with a VG-Instruments ZAB 2-SE-FDP. The elemental analyses were carried out by the Microanalytical Laboratory of Johannes Gutenberg University. The UV–vis−NIR absorption measurements were performed on a Perkin-Elmer Lambda 15 spectrophotometer and the PL measurements on a SPEX Fluorolog 2 type F212 steady-state fluorometer. Cyclic voltammetry and differential pulse voltammetry were performed on an EG&G Princeton Applied Research potentiostat, model 273, in a solution of Bu_4NPF_6 (0.1 M) in dry dichloromethane with a scan rate of 50 mV/s at room temperature under argon. A platinum electrode was used as the working electrode, an Ag/AgCl electrode as the reference electrode, and a platinum wire as the counter electrode.

Quantum Chemical Calculations. Density functional theory (DFT) calculations were performed with the Turbomole program suite version 5.7. Geometry optimizations were carried out with the BP86 functional making use of the RI approximation. The ionization potential (IP) was derived from a single point energy (BP86) of the positively charged radical cation at the relaxed geometry of the neutral dye molecule. Vertical optical excitation energies were obtained from time-dependent DFT (TDDFT) calculations at the B3LYP level. The def-SV(P) basis set was applied in all calculations. Methods: HOMO energy: $E^{(\text{cation})}_{(\text{single-point energy})} - E^{(\text{neutral})}_{(\text{optimized})}$ using P86/def-SV(P). LUMO energy: HOMO energy + optical excitation energy (TDDFT). HOMO/LUMO pictures: B3-LYP/def-SV(P)//BP86/def-SV(P).

DSSC Fabrication and Characterization. FTO (fluorine-doped tin oxide)-coated glass sheets with 25 mm × 15 mm × 3 mm size (Nippon Sheet Glass) were used as substrate. Before use, the glass sheets were successively treated for 5 min in an ultrasonic bath with RBS 35 0.5% cleaning solution, deionized water, and twice with acetone, boiled twice in 2-propanol for 5 min, and finally dried with flowing nitrogen. Liquid cells: nanostructured TiO_2 photoelectrodes were prepared by blading a colloidal solution (20 nm sized anatase particles) onto a conducting glass (Nippon Sheet glass, 10 Ω/square) and sintered for 30 min at 450 °C. The 10 μm thick TiO_2 electrodes were then immersed into 0.5 M dye in DCM overnight. The counter electrodes were made by adding a Pt solution (5 mM H_2PtCl_6 in 2-propanol) on a conducting glass and heating for 15 min at 380 °C, forming a light gray surface of nanoparticulate platinum on the conducting glass. The cells were sealed with a frame of Surlyn SX1170 by heating the clamped device at 120 °C for 7 min. Solid cell: a 15 nm TiO_2 compact blocking layer was made by argon-sputtering Ti on the substrates; on top of this layer a 1.8 μm thick porous TiO_2 film was applied by spin-coating a TiO_2 paste (CCIC) with 20 nm particle size for 30 s at 4500 rpm. After this, the substrates were sintered in the oven (45 min heating up from room temperature to 450 °C and then 30 min at 450 °C): The samples were cooled down and put overnight in a 0.5 mM dye solution; the day after they were rinsed with the dye solution solvent, dried first with flowing nitrogen and then in a vacuum oven at 40 °C for 4 h. The next step was spin-coating at 2000 rpm for 30 s with the p-conductor solution, waiting 60 s after the wetting of the surface to allow pore filling; the solution was prepared in the glovebox, using chlorobenzene as solvent, and contained Spiro-MeOTAD (Merck, 0.16 M), lithium salt ($LiN(SO_2CF_3)_2$, Fluka, 15 mM), and 4-*tert*-butylpyridine (Aldrich, 60 mM). The substrates were dried in a vacuum oven at 40 °C for 4 h. A 30 nm gold back-electrode was thermally evaporated in vacuum. The spectral photoresponse was measured with a xenon arc lamp (LOT LSB510) and a monochromator (ACTON SpectraPro-2150i) while monitoring the illumination intensity. The measurements were performed with 100 mW cm^{-2} biased white light. The overall solar-to-energy conversion efficiencies (η) were measured under Air Mass 1.5 (AM1.5) conditions using a 300 W xenon arc lamp (LOT LSB 530), calibrated with a reference Si solar cell.

Material Synthesis. All chemicals and reagents were used as received from commercial sources without further purification. Solvents for chemical synthesis were purified or freshly distilled prior to use according to standard procedures. All chemical reactions were carried out under an inert atmosphere. Intermediate dibromopentaphenylene **4** were synthesized according to previous work in our group.[15]

Synthesis of the Aldehyde 5. Under a nitrogen atmosphere and at −78 °C, n-BuLi (0.63 mL, 1.6 M in hexane) was added dropwise to a dry tetrahydrofuran (40 mL) solution containing **4** (1.79 g, 1 mmol). After 30 min stirring, 0.2 mL of *N*-methylformamide was added slowly to the reaction solution. The temperature of the solution was brought back to room temperature, and after another 4 h stirring, the reaction was quenched with 2 N HCl. The solution was extracted with ethyl acetate and subjected to flash column chromatography (silica gel, toluene/hexane = 1:4). A light yellow solid was obtained with a yield of 41% (710 mg). ^{1}H NMR (250 MHz, CD_2Cl_2): δ (ppm): 10.01 (s, 1H), 7.85–7.64 (m, 10H), 7.50–7.39 (m, 2H), 7.23 (d, 8H, J = 8.2 Hz), 7.13 (d, 8H, J = 8.0 Hz), 2.57 (t, 8H, J = 7.5 Hz), 2.03 (t, 8H), 1.58 (t, 8H), 1.28–1.05 (m, 80H), 0.88–0.75 (m, 16 H), 0.61 (b, 8H). ^{13}C NMR (75 MHz, CD_2Cl_2) δ (ppm): 192.3, 153.8, 152.7, 152.6, 152.5, 152.2, 152.0, 151.9, 151.7, 151.5, 151.2, 150.8, 147.8, 143.8, 143.7, 143.6, 142.0, 141.9, 141.7, 141.6, 141.3, 141.1, 140.8, 140.5, 140.2, 139.9, 139.8, 139.6, 135.6, 130.3, 130.1, 128.7, 128.5, 123.5, 121.1, 120.2, 118.7, 118.1, 115.2, 115.1, 64.8, 55.4, 40.9, 40.8, 35.8, 32.2, 32.1, 31.9, 30.4, 30.3, 29.8, 29.6, 24.2, 23.0, 22.9, 14.2. Elemental analysis

(21) Shibano, Y.; Umeyama, T.; Matano, Y.; Imahori, H. *Org. Lett.* **2007**, *9*, 1971.

for $C_{123}H_{165}BrO$: Calculated: (%) C, 84.93, H, 9.56. Found: (%) C, 85.72, H, 9.48. FDMS: *m/z* 1738.1.

Synthesis of Amine 6. Under a nitrogen atmosphere, a mixture of **5** (200 mg, 0.12 mmol), diphenylamine (100 mg, 0.5 mmol), $Pd(OAc)_2$ (2 mg, 0.009 mmol), P(*t*-Bu)$_3$ (4 mg, 0.018 mmol), and Cs_2CO_3 (88 mg, 0.27 mmol) in toluene (10 mL) was stirred and heated at 80 °C for 8 h. After cooling to room temperature, saturated ammonium chloride solution was added to the reaction solution. The solution was extracted with ethyl acetate and subjected to flash column chromatography (silica gel, toluene/hexane = 1:4). An orange solid was obtained with a yield of 74% (160 mg). ^{1}H NMR (300 MHz, CD_2Cl_2) δ (ppm): 9.92 (s, 1H), 7.75–7.66 (m, 7H), 7.55 (s, 1H), 7.46 (s, 1H), 7.36 (s, 1H), 7.17 (d, 8H, J = 8.1 Hz), 7.01 (d, 8H, J = 8.4 Hz), 6.91 (d, 5H, J = 8.4 Hz), 6.89 (d, 5H, J = 7.8 Hz), 2.47 (t, 8H, J = 8.1 Hz), 2.21 (s, 6H), 1.98 (t, 4H), 1.82 (t, 4H), 1.47 (t, 8H), 1.06–0.97 (m, 80H), 0.77–0.60 (m, 32H). ^{13}C NMR (75 MHz, CD_2Cl_2) δ (ppm): 192.3, 152.7, 152.6, 152.4, 152.2, 152.0, 151.8, 151.0, 148.0, 147.8, 147.7, 145.9, 143.9, 143.7, 142.0, 141.9, 141.7, 141.6, 141.3, 139.7, 139.6, 138.6, 135.7, 135.5, 132.5, 132.4, 130.3, 130.1, 129.7, 128.7, 128.5, 125.3, 124.8, 124.4, 123.6, 123.5, 122.6, 120.5, 120.2, 118.7, 118.5, 118.1, 118.0, 117.6, 116.7, 115.1, 114.9, 64.7, 55.4, 55.1, 40.8, 35.8, 32.2, 32.1, 31.9, 30.4, 30.3, 30.0, 29.8, 29.7, 29.6, 29.5, 24.3, 24.2, 23.0, 22.9, 20.8, 14.2. Elemental analysis for $C_{137}H_{179}NO$: Calculated: (%) C, 88.66, H, 9.72, N, 0.75. Found: (%) C, 88.00, H, 10.07, N, 0.39. FD-mass: *m/z* 1855.1.

Synthesis of Dye 1. A mixture of **6** (70 mg, 0.037 mmol), cyanoacetic acid (10 mg, 0.12 mmol), ammonium acetate (2 mg, 0.026 mmol), and acetic acid (10 mL) was heated at 130 °C for 5 h. After cooling to room temperature, it was precipitated by pouring into ethanol. The resulting solid was filtered, washed thoroughly with water and methanol, and reprecipitated from dichloromethane by pouring into methanol to give a orange solid (62 mg, 86%). ^{1}H NMR (250 MHz, CD_2Cl_2) δ (ppm): 8.27 (s, 1H), 7.93 (d, 2H), 7.76 (s, 1H), 7.71 (s, 1H), 7.67 (m, 3H), 7.56 (s, 1H), 7.47 (s, 1H), 7.36 (m, 1H), 7.14 (d, 8H, J = 8.0 Hz), 7.05 (d, 8H, J = 8.2 Hz), 6.96 (d, 5H, J = 8.2 Hz), 6.89 (d, 4H, J = 8.2 Hz), 6.80 (d, 1H, J = 8.2 Hz), 2.49 (t, 8H, J = 7.5 Hz), 2.22 (s, 6H), 1.99 (t, 4H), 1.82 (t, 4H), 1.17–0.89 (m, 80H), 0.78–0.60 (m, 32 H). ^{13}C NMR (75 MHz, CD_2Cl_2) δ (ppm): 152.8, 152.6, 152.4, 152.1, 152.0, 151.8, 151.1, 148.0, 146.0, 145.9, 143.9, 143.7, 142.0, 141.9, 141.6, 141.5, 141.2, 140.0, 139.7, 138.7, 135.7, 132.5, 131.2, 130.2, 130.1, 128.9, 128.7, 128.5, 125.5, 124.4, 122.6, 120.5, 120.4, 118.6, 118.4, 118.0, 117.6, 116.7, 115.1, 114.9, 64.7, 40.8, 35.8, 32.2, 32.1, 31.8, 30.4, 30.0, 29.8, 29.7, 29.6, 29.4, 24.4, 24.3, 23.0, 22.9, 20.8, 14.2. Elemental analysis for $C_{140}H_{180}N_2O_2$: Calculated: (%) C, 87.44, H, 9.43, N, 1.46. Found: (%) C, 87.88, H, 9.73, N, 1.03. MALDI-TOF: *m/z* 1922.2.

Synthesis of Compound 7. Under a nitrogen atmosphere, a mixture of **5** (200 mg, 0.12 mmol), phenothiazine (100 mg, 0.5 mmol), $Pd(OAc)_2$ (2 mg, 0.009 mmol), P(*t*-Bu)$_3$ (4 mg, 0.018 mmol), and Cs_2CO_3 (88 mg, 0.27 mmol) in toluene (10 mL) was stirred and heated at 80 °C for 8 h. After cooling to room temperature, saturated ammonium chloride solution was added to the reaction solution. The solution was extracted with ethyl acetate and subjected to flash column chromatography (silica gel, toluene/hexane = 1:4). A yellow orange solid was obtained with a yield of 63% (135 mg). ^{1}H NMR (300 MHz, CD_2Cl_2) δ (ppm): 9.92 (s, 1H), 7.78–7.66 (m, 11 H), 7.27 (s, 1H), 7.18 (d, 8H, J = 8.4 Hz), 7.06 (d, 8H, J = 8.4 Hz), 6.91 (m, 2H), 6.70 (b, 4H), 6.12 (b, 2H), 2.49 (t, 8H, J = 6.9 Hz), 1.96 (t, 8H), 1.51 (t, 8H), 1.17–0.98 (m, 80H), 0.79–0.67 (m, 32H). ^{13}C NMR (75 MHz, CD_2Cl_2) δ (ppm): 192.4, 154.3, 152.7, 152.6, 152.0, 151.6, 147.7, 144.9, 143.7, 143.6, 142.0, 142.0, 141.6, 141.6, 140.8, 140.6, 140.2, 140.2, 139.9, 139.7, 135.6, 128.7, 128.5, 127.2, 126.8, 122.6, 119.8, 116.0, 115.2, 64.8, 64.8, 55.6, 55.4, 40.9, 4.08, 35.8, 32.2, 32.1, 31.8, 30.3, 29.8, 29.8, 29.7, 29.6, 29.5, 24.5, 24.3, 23.0, 22.9, 14.2. Elemental analysis ($C_{135}H_{173}NOS$): Calculated: (%) C, 87.27, H, 9.39, N, 0.75, S, 1.73. Found: (%) C, 86.80, H, 9.22, N, 0.55, S, 163. FD-mass: *m/z* 1857.1.

Synthesis of Dye 2. A mixture of **7** (120 mg, 0.065 mmol), cyanoacetic acid (20 mg, 0.23 mmol), ammonium acetate (5 mg, 0.065 mmol), and acetic acid (10 mL) was heated at 130 °C for 5 h. After cooling to room temperature, it was precipitated by pouring into ethanol. The resulting solid was filtered, washed thoroughly with water and methanol, and reprecipitated from dichloromethane by pouring into methanol to give a yellow solid (100 mg, 81%). ^{1}H NMR (250 MHz, CD_2Cl_2) δ (ppm): 8.28 (s, 1H), 7.94 (m, 2H), 7.79 (m, 3H), 7.68 (m, 5H), 7.28 (s, 1H), 7.19 (d, 9H, J = 7.5 Hz), 7.06 (d, 8H, J = 7.5 Hz), 7.91 (m, 2H), 6.71 (m, 4H), 6.12 (m, 2H), 2.49 (t, 8H, J = 7.5 Hz), 1.99 (t, 8H), 1.51 (t, 8H), 1.17–0.98 (m, 80H), 0.78–0.68 (m, 32 H). ^{13}C NMR (75 MHz, CD_2Cl_2) δ (ppm): 153.8, 152.7, 152.4, 152.3, 151.8, 151.7, 151.0, 150.8, 147.9, 146.0, 143.9, 143.8, 141.9, 141.8, 141.5, 140.9, 140.6, 140.4, 140.2, 139.9, 138.8, 137.5, 135.7, 132.5, 131.6, 130.1, 128.7, 128.5, 126.5, 124.4, 121.3, 121.0, 120.5, 118.6, 117.8, 117.5, 116.7, 64.7, 40.9, 35.9, 32.2, 32.1, 31.9, 30.4, 30.3, 29.9, 29.8, 29.7, 29.6, 24.3, 24.2, 23.0, 22.9, 20.8, 14.2. Elemental analysis for $C_{138}H_{174}N_2O_2S$: Calculated: (%) C, 86.11, H, 9.11, N, 1.46, S, 1.67. Found: (%) C, 85.22, H, 9.16, N, 1.19, S, 1.99. MALDI-TOF: *m/z* 1924.1.

Synthesis of Amine 8. Under a nitrogen atmosphere, a mixture of **5** (160 mg, 0.092 mmol), bindschedler's green (40 mg, 0.157 mmol), $Pd(OAc)_2$ (2 mg, 0.009 mmol), P(*t*-Bu)$_3$ (4 mg, 0.018 mmol), and Cs_2CO_3 (88 mg, 0.27 mmol) in toluene (10 mL) was stirred and heated at 80 °C for 8 h. After cooling to room temperature, saturated ammonium chloride solution was added to the reaction solution. The solution was extracted with ethyl acetate and subjected to flash column chromatography (silica gel, ethyl acetate/dichloromethane = 0–5%. An orange solid was obtained with a yield of 54% (95 mg). ^{1}H NMR (250 MHz, TDF) δ (ppm): 9.92 (s, 1H), 7.94 (s, 1H), 7.94–7.35 (m, 9H), 7.20 (d, 8H, J = 8.2 Hz), 7.01 (d, 8H, J = 8.0 Hz), 6.90 (d, 4H, J = 6 Hz), 6.62 (d, 2H, J = 8.2 Hz), 6.52 (d, 4H, J = 8.5 Hz), 2.88 (s, 12H), 2.54 (t, 8H, J = 7.7 Hz), 2.07–1.88 (m, 8H), 1.55 (m, 8H), 1.30–1.08 (m, 80H), 0.89–0.80 (m, 24H). ^{13}C NMR (75 MHz, TDF) δ (ppm): 192.3, 153.7, 151.9, 151.7, 151.5, 151.1, 143.6, 143.4, 141.6, 140.4, 140.3, 130.6, 130.2, 129.9, 127.9, 127.5, 127.4, 125.3, 125.2, 124.5, 119.7, 118.1, 117.5, 115.4, 112.9, 101.3, 63.9, 54.5, 53.9, 39.6, 35.0, 31.4, 31.3, 31.2, 29.7, 29.6, 29.1, 29.0, 28.9, 28.8, 28.7, 28.6, 24.5, 24.2, 23.9, 23.7, 23.6, 23.3, 22.1, 22.0, 13.0. FD-mass: *m/z* 1912.5.

Synthesis of Dye 3. A mixture of **8** (90 mg, 0.047 mmol), cyanoacetic acid (20 mg, 0.23 mmol), ammonium acetate (5 mg, 0.065 mmol), and acetic acid (10 mL) was heated at 130 °C for 5 h. After cooling to room temperature, it was precipitated by pouring into ethanol. The resulting solid was filtered, washed thoroughly with water and methanol, and reprecipitated from dichloromethane by pouring into methanol to give crimson solid (65 mg, 70%). ^{1}H NMR (250 MHz, TDF) δ (ppm): 8.30 (s, 1H), 8.17 (s, 1H), 7.99–7.74 (m, 7H), 7.58 (s, 1H), 7.38 (d, 1H, J = 8.2 Hz), 7.26 (d, 8H, J = 8.0 Hz), 7.07 (d, 8H, J = 6 Hz), 6.96 (d, 5H, J = 8.7 Hz), 6.66 (d, 1H, J = 8.7 Hz), 6.55 (d, 4H, J = 8.5 Hz), 2.89 (s, 12H), 2.55 (t, 8H, J = 7.5 Hz), 2.07–1.87 (m, 8H), 1.59 (m, 8H), 1.32–1.08 (m, 80H), 0.88–0.80 (m, 24H). ^{13}C NMR (75 MHz, TDF) δ (ppm): 162.7, 153.7, 151.8, 151.7, 151.5, 151.3, 151.1, 149.9, 146.6, 146.0, 143.6, 143.5, 143.4, 141.6, 140.9, 140.4, 140.3, 138.8, 138.7, 137.8, 137.7, 135.2, 130.2, 129.9, 128.1, 127.9, 127.6, 127.5, 127.4, 125.2, 125.1, 124.5, 119.7, 119.5, 118.1, 117.5,

116.8, 115.7, 115.4, 114.0, 113.7, 112.9, 101.3, 63.9, 54.4, 53.9, 39.8, 39.6, 39.4, 35.0, 31.4, 31.3, 31.2, 31.1, 29.7, 29.6, 29.3, 29.2, 29.1, 29.0, 28.9, 28.8, 28.6, 25.3, 25.1, 25.0, 24.8, 24.6, 24.4, 24.2, 23.9, 23.6, 23.5, 23.4, 23.1, 22.3, 22.2, 22.1, 22.0, 21.9, 13.0. Elemental Analysis for $C_{142}H_{186}N_4O_2$: Calculated: (%) C, 86.09, H, 9.46, N, 2.83. Found: (%) C, 85.27, H, 9.23, N, 2.36. MALDI-TOF mass: *m*/*z* 1980.3.

Acknowledgment. This work was financially supported by the Bundesministerium für Bildung and Forschung (Projects 13N8165 OLAS and 13N8215 OLED), BASF AG and Dupont Displays. G. Zhou gratefully acknowledges the Alexander von Humboldt Stiftung for the grant of a research fellowship.

CM703459P